doi:10.1093/brain/aws243 Brain 2012: 135; 3039–3050 | 3039

BRAIN
A JOURNAL OF NEUROLOGY

Amyloid-β-dependent compromise of microvascular structure and function in a model of Alzheimer's disease

Adrienne Dorr,[1] Bhupinder Sahota,[1] Lakshminarayan V. Chinta,[1,4] Mary E. Brown,[2] Aaron Y. Lai,[2] Keran Ma,[2] Cheryl A. Hawkes,[3] JoAnne McLaurin[2] and Bojana Stefanovic[1,4]

1 Sunnybrook Research Institute, 2075 Bayview Avenue, Toronto, Ontario, Canada M4N 3M5
2 Department of Laboratory Medicine and Pathobiology, University of Toronto, 1 King's College Circle Toronto, Ontario, Canada M5S 1A8
3 Division of Clinical Neurosciences, Southampton General Hospital, University of Southampton, South Lab and Pathology Block, LD66 (Mailpoint 806), Tremona Road Southampton, Hampshire SO16 6YD, UK
4 Department of Medical Biophysics, University of Toronto, 610 University Avenue, Toronto, Ontario, Canada M5G 2M9

Correspondence to: JoAnne McLaurin, PhD
Department of Laboratory Medicine and Pathobiology,
University of Toronto,
1 King's College Circle Toronto,
Ontario,
Canada M5S 1A8
E-mail: j.mclaurin@utoronto.ca

The majority of patients with Alzheimer's disease have cerebral amyloid angiopathy, thus showing deposition of amyloid-β peptides in the walls of leptomeningeal and cortical arterioles. These deposits are believed to result from impaired clearance of parenchymal amyloid-β peptides. In the current work, we examined the changes in cortical microvascular structure and function *in situ* in TgCRND8, a transgenic mouse model of Alzheimer's disease. In contrast to venules, cortical arterioles were shown to increase in tortuosity and decrease in calibre with amyloid-β peptide accumulation. These structural changes were accompanied by progressive functional compromise, reflected in higher dispersion of microvascular network transit times, elongation of the transit times, and impaired microvascular reactivity to hypercapnia in the transgenic mice. Moreover, inhibition of amyloid-β peptide oligomerization and fibrillization via post-weaning administration of *scyllo*-inositol, a naturally occurring stereoisomer of *myo*-inositol, rescued both structural and functional impairment of the cortical microvasculature in this Alzheimer's disease model. These results demonstrate that microvascular impairment is directly correlated with amyloid-β accumulation and highlight the importance of targeting cerebrovascular amyloid angiopathy clearance for effective diagnosis, monitoring of disease progression and treatment of Alzheimer's disease.

Keywords: cerebral amyloid angiopathy; vessel tortuosity; microvasculature; two-photon fluorescence microscopy; scyllo-inositol

Introduction

Alzheimer's disease, the most common cause of dementia, involves a progressive decline in memory and cognition that correlates with synaptic and neuronal dysfunction and loss (Querfurth and LaFerla, 2010). In addition to amyloid-β peptide-containing extracellular plaques, intracellular neurofibrillary tangles and atrophy in select brain areas (Collie and Maruff,

Received March 1, 2012. Revised May 31, 2012. Accepted July 13, 2012

2000; Citron, 2002), Alzheimer's disease is associated with cerebrovascular changes that precede clinical symptoms of the disease, worsen over the course of degeneration, and exacerbate cognitive decline (Nicolakakis and Hamel, 2011). The latter are evidenced by amyloid deposition on the walls of leptomeningeal and cortical penetrating arteries (cerebral amyloid angiopathy), inhibition of angiogenesis, impaired vascular tone, resting hypoperfusion and reduced haemodynamic responses to stimulation (Miao *et al*., 2005; Girouard and Iadecola, 2006; Shin *et al.,* 2007; Takano *et al*, 2007). Post-mortem histology has shown various changes in blood vessel morphology in the Alzheimer's disease brain: decreased vascular density, increased vessel curvature (Fischer *et al.,* 1990), degeneration of smooth muscle cells, vascular endothelium alterations (Kalaria, 1996, 2002), capillary fragmentation and abnormal blood–brain barrier permeability (Perlmutter, 1994). Clinically, the degree of cerebral amyloid angiopathy is associated with cognitive impairment (Pfeifer *et al.,* 2002), white matter hyperintensities (Holland *et al*., 2008) and cortical infarcts (Greenberg, 2002). Although cerebral amyloid angiopathy-related vascular impairments have been reported in both patients and mouse models, it is still unclear whether this relationship is correlative or causative. Furthermore, the development of cerebral amyloid angiopathy in a brain region specific manner suggests that mechanisms identified to date do not account for the specificity of deficits in human patients.

Deposition of amyloid-β within the vascular space is the result of an age- and/or disease-associated failure of elimination of amyloid-β from the parenchyma to the periphery for degradation (Weller *et al*., 2009). There are multiple mechanisms proposed for efflux of amyloid-β, including the active transport of amyloid-β across the blood–brain barrier to the plasma by lipoprotein receptor-related protein 1 (Deane *et al*., 2004; Bell *et al*., 2009). Alternatively, other studies have shown active ingestion of amyloid-β by perivascular macrophages, smooth muscle and endothelial cells within the vessel wall, followed by amyloid-β degradation within the lysosomal pathway (Deane *et al*., 2004; Hawkes and McLaurin, 2009). In addition, perivascular lymphatic drainage of amyloid-β along the basement walls of arteries and capillaries to peripheral lymph nodes is another route for peripheral degradation (Weller *et al*., 2009).

In light of the wealth of evidence that the aggregation of soluble amyloid-β peptides contributes to neuronal dysfunction in Alzheimer's disease, numerous compounds have been developed to prevent amyloid-β oligomerization and/or fibrillization (LeVine, 2007). In particular, incubation of amyloid-β_{42} with scyllo-inositol blocks fibril formation, stabilizes small amyloid-β oligomers, rescues amyloid-β_{42}-induced cell toxicity and attenuates amyloid-β oligomer-induced inhibition of hippocampal long-term potentiation (McLaurin *et al*., 2000; Townsend *et al*., 2006). Moreover, both prophylactic and therapeutic oral administration of scyllo-inositol reduces high-molecular-weight amyloid-β oligomers and cortical plaque load in the TgCRND8 mouse model of Alzheimer's disease (McLaurin *et al.,* 2006). Magnetic resonance spectroscopy demonstrated region-specific delivery of scyllo-inositol in two mouse models of Alzheimer's disease after dietary supplementation, with scyllo-inositol delivery to the cortex and hippocampus in both models (Choi *et al.,* 2010). Therefore, this CNS bioavailable small molecule can now be utilized to probe the relationship between amyloid-β accumulation and the cerebral vasculature changes seen in post-mortem Alzheimer's disease brains (Fenili *et al.,* 2011). Previous studies have demonstrated cerebrovascular dysfunction in young and old transgenic models of Alzheimer's disease as a function of amyloid-β (Miao *et al*., 2005; Shin *et al*., 2007; Han *et al.,* 2008). To date, however, these changes have not been correlated with *in situ* determination of vessel morphological alterations. Furthermore, the implications of the potential cerebral amyloid angiopathy treatments on vessel morphology and function have not been fully elucidated. Vascular side effects have been reported for most amyloid-β peptide targeting strategies in short-term treatment of patients with Alzheimer's disease; however, the long-term effects on the vascular structure and function, once cerebral amyloid angiopathy is cleared, are still unknown.

The present work examined the progression of changes in the cortical microvascular morphology and function with and without scyllo-inositol treatment in the TgCRND8 mouse model of Alzheimer's disease, which exhibits a pattern of vascular amyloid deposition typically found in human cerebral amyloid angiopathy. The amyloid-β deposition in capillary beds leading to degenerated string capillaries (Hunter *et al*., 2012) versus amyloid-β deposition surrounding larger arterioles and arteries may have differential effects on vascular function. The use of a mouse model of overproduction of amyloid-β allows us to address the role of amyloid-β in effecting changes in arteriolar morphology that lead to functional deficits. *In vivo* two-photon laser scanning microscopy and *ex vivo* immunohistochemistry were used to elucidate the influence of disease progression on the cortical penetrating vessels morphology, microvascular network efficiency and vascular reactivity to hypercapnia. To demonstrate a direct role for amyloid-β in vascular alterations, we utilized scyllo-inositol treatment to remove amyloid-β at various stages of amyloid deposition.

Materials and methods

Mice

TgCRND8/129/SvJ ($n = 42$) overexpressing human Swedish (KM670/671NL) and Indiana (V717F) amyloid precursor protein mutations under a hamster prion protein promoter were maintained on a 129 background (Chishti *et al.,* 2001). Early onset amyloid-β deposition and cognitive deficits have been shown in transgenic mice expressing a double mutant form of amyloid precursor protein. Mice were matched for age and sex and allowed food and water *ad libitum*. The transgenic and their non-transgenic littermates ($n = 32$) were divided into three cohorts based on the amyloid-β accumulation in the transgenic group: 2–3 months of age with early soluble amyloid-β and little to no plaque load; 4–6 months of age with moderate soluble amyloid-β and plaque load; and 7–12 months of age with extensive soluble amyloid-β and heavy plaque load similar to end-stage human Alzheimer's disease (henceforth referred to as early, mid and late stage, respectively). A subset of transgenic mice ($n = 15$) were given scyllo-inositol in drinking water (10 mg/ml) for 4 weeks (for the mid stage cohort) and *ad libitum* from weaning (for the late stage cohort) up to the imaging time point. Non-transgenic, transgenic

or scyllo-inositol-treated transgenic mice were imaged at the latter two stages. All experimental protocols were approved by Sunnybrook Research Institute Animal Care Committee and comply with the requirements set forth by the Canadian Council for Animal Care.

Brain tissue preparation and thioflavin S staining

Transgenic and non-transgenic mice were deeply anaesthetized with an overdose of sodium pentobarbital and perfused intracardially with PBS (0.01 M), followed by 10% formalin. Brains were sectioned (20 mm), washed in PBS, and incubated for 5 min at room temperature with 1% thioflavin S (Sigma-Aldrich). Tissues were differentiated twice in 70% ethanol, washed in PBS and mounted under a coverslip with anti-fading agent. Photomicrographs were captured using a Coolsnap digital camera (Photometrics) mounted on a Zeiss Axioscope 2 Plus microscope and exported to Photoshop CS.

Cortical blood vessel isolation and biochemical analyses

Cortical blood vessel isolation was performed as previously described (Hawkes and McLaurin, 2009). Briefly, brain homogenates were centrifuged (100 000*g*, 1 h, 4°C), and pellets resuspended in 500 ml of 0.1 M ammonium carbonate + 7% SDS (plus protease inhibitor cocktail) and stirred for ~4 h. Tissues were filtered through 100 μm and 40 μm mesh filters to isolate blood vessel tufts from cortical filtrate. Tissues were sonicated in 70% formic acid, centrifuged (100 000*g*, 1 h, 4°C) and neutralized. Neutralized samples were diluted and analysed using commercially available sandwich ELISA kits, following manufacturer's instructions (BioSource).

Surgical preparation

Surgical procedures were similar to those described in detail previously (Lindvere *et al.*, 2010). Briefly, mice were anaesthetized via inhalation of isoflurane [5% induction 1.5–2% maintenance in oxygen enriched medical air (32% oxygen, balance nitrogen)]. Body temperature was kept at 37.5°C, using a rectal probe and a feedback-controlled heating pad (TC-1000, CWE Inc.). Hydration was maintained with subcutaneous injections of 0.5–1.0 ml Ringer's solution every hour. Animals were placed in a stereotaxic frame, with the head secured by ear and incisor bars. A small cranial window, ~3 mm in diameter, was centred at 1.5 mm medial–lateral and −0.5 mm anterior–posterior relative to bregma. The dura was removed and the space between the skull surface and brain surface filled with 1% agarose in PBS (Sigma-Aldrich). The cranial window was closed with a 5-mm circular glass coverslip (World Precision Instruments) secured to the surrounding skull with cyanoacrylate adhesive, and the dental cement-based well around the cranial window filled with double-distilled water, for the water-dipping objective. A subset of animals ($n = 17$) were tracheotomized and mechanically ventilated (SAR 830/P, CWE Inc.) for the bolus-tracking experiments, so as to allow estimation of vascular transit times during a hypercapnic challenge (10% carbon dioxide in the inspired gas mixture) and thus provide a measure of vascular reactivity and function. End-tidal respiratory pressure, temperature, oxygen saturation, breath and pulse distention and heart rate were recorded throughout surgery and imaging (Biopac MP150, Biopac Systems Inc.; MouseOx, Starr Life Sciences Corp.).

Image acquisition

To allow imaging of the vasculature, a tail vein catheter was implanted for the injection of 1.5–2.0 ml of fluorescent dextran (70 kDa Texas Red or 70 kDa Oregon Green 33 mg/kg, dissolved in PBS; Invitrogen). The animal was positioned under a ×25 1.05 NA objective with a working distance of 2 mm (Olympus), and the animal and stage rotated to render the exposed cortical surface horizontal. Scanning was performed with an FV1000MPE multiphoton laser scanning microscope (Olympus). A Mai Tai Titanium Sapphire tunable laser (690–1040 nm; Newport Corp.) was used to excite the fluorescent dextran at 810 nm. An external photomultiplier tube (Hamamatsu) collected the resulting fluorescent emissions.

Four bolus injections of 30 μl (8.25 mg/kg, for a total of 33 mg/kg) of the fluorescent dextran were administered via the tail vein catheter to estimate vascular transit times both during normocapnia and in the course of hypercapnia (Lindvere *et al.*, 2010). Time series scans were acquired during each bolus at a single transverse plane at varying depths (256 pixels × ~128 pixels, 2 μm/pixel, 2 μs/pixel, for a total scan time per bolus tracking acquisition of 60 s). A stack of XY scans (0.5–1.0 μm × 0.5–1.0 μm), every 1.5 μm, spanning 300–650 μm of the cortex were obtained for each mouse over a 512 μm × 512 μm field of view parallel to the cortical surface (dwell time 4–8 μs/pixel, total scan time of 10–75 min depending on imaging parameters and the range of cortical depths imaged). Plaques were visualized using the intrinsic autoflourescent emissions (Kwan *et al.*, 2009).

Morphological data analysis

Penetrating vessels were identified as those being 10 μm in diameter or more that descended into the cortex roughly perpendicular to the surface of the brain. Semi-automatic intensity-based vessel segmentation was performed using Imaris (Bitplane). The degree of curvature (tortuosity) was defined by the length along the vessel between beginning and endpoints, divided by the 3D Euclidian distance between beginning and endpoints (Bullitt *et al.*, 2003). A higher value thus indicated a more tortuous vessel, while a perfectly straight vessel would have been assigned a tortuosity value of 1. The average cross-sectional area of the vessels was determined by dividing the vessel volume by vessel length, and the average vessel radius calculated from this average cross-sectional area. Penetrating vessels were designated arteries or veins based on their morphological features and branching pattern (Scharrer, 1940; Duvernoy *et al.*, 1981; Kasischke *et al.*, 2011). Those cortical penetrating vessels exhibiting few branches across the cortical depth, having a large capillary-free space in their surround and having a fairly constant diameter throughout their length were designated as arteries. In turn, vessels showing more branches, a smaller capillary free space in their surround, and a diameter that increased toward the cortical surface were deemed venules. Validation of vessel designation was done using the bolus-tracking data since venules exhibit delayed bolus arrival times relative to the arterioles.

Bolus-tracking data analysis

The bolus time series data acquired during normocapnia and hypercapnia were 2D median filtered (3 × 3 voxel kernel in x and y). Maximum intensity projection was performed on the filtered time series and the vessels of interest segmented semi-automatically. For every vessel thus identified, the corresponding average vessel signal intensity time series were computed, normalized to the peak signal intensity, and integrated over time. The bolus passage, during both

normocapnia and hypercapnia, was next modelled using the gamma variate function (Kim *et al*., 2010; Kershaw and Cheng, 2011), following our earlier work (Stefanovic *et al*., 2008), the average vessel signal intensity changes with time were thus modelled as

$$S(t) = A(t/\mathrm{TTP})^{a} \exp(-(t - \mathrm{TTP}/\beta))$$

with

$$\alpha = \mathrm{TTP}^2/\mathrm{FWHM}^2 * 8\log 2$$
$$\beta = \mathrm{FWHM}^2/\mathrm{TTP}/8/\log 2$$

where A is a scaling constant, TTP is the time to peak, FWHM is the full-width at half-maximum, and t is the time.

Statistical analysis

All data were analysed using linear mixed effects analysis (lme function in nlme package, R), with subjects treated as random variables, thus allowing for within-subject errors to be correlated. This modelling produces sensible restricted maximum likelihood estimates from the unbalanced allocation of subjects by factor (Pinheiro and Bates, 2000). For the ELISA measurements, we thus investigated the dependence of the amyloid-$\beta_{40,42}$ load on the two fixed effects of interest: tissue type (blood vessel versus vessel-depleted cortex) and age (in days). For the vessel morphology measurements, tortuosity, average radius and vessel length were modelled as linear mixed effects functions of state (non-transgenic, transgenic and scyllo-inositol-treated transgenic) and age (in days) or stage of amyloid-β accumulation (early, middle or late) for each vessel type (arterioles and venules). Similarly, we investigated the effect of state and age on vascular transit time (in s) and the hypercapnia-elicited changes in vascular transit time (in s). In these, subjects, vessels and bolus repetition were treated as nested random effects. Finally, we used an *F*-test to compare the variance (i.e. dispersion) of the vascular transit times between non-transgenic, transgenic and scyllo-inositol-treated transgenic cohorts.

Results

Amyloid-$\beta_{40,42}$ vessel load progressively increases with age

We have previously shown that stable, soluble oligomeric amyloid-β_{40} and amyloid-β_{42} accumulate in the cortex of TgCRND8 mice (transgenic) with age, in association with extracellular plaque deposition (Ma *et al*., 2011). To evaluate the temporal development of cerebral amyloid angiopathy in this mouse model, brain tissue sections from 2- to 3- (early stage cerebral amyloid angiopathy), 4- to 6- (mid-stage cerebral amyloid angiopathy) and 7- to 12-month-old (late-stage cerebral amyloid angiopathy) transgenic mice were stained with thioflavin S dye. As shown in Fig. 1, amyloid-β deposition in the young mice was detected predominantly in parenchymal plaques, with very little thioflavin S observed on the blood vessels (Fig. 1A and D). By 4 months of age, numerous amyloid-positive cortical blood vessels were visible in the field of view (×25 magnification, Fig. 1B and E). In the aged mice, both the number of vessels with cerebral amyloid angiopathy and the extent of amyloid-β deposition along the vessel wall were increased compared with mice in the early and mid-stage cerebral amyloid angiopathy (Fig. 1C and F). To quantify the age-dependent increase in cerebral amyloid angiopathy in relation to amyloid-β accumulation in the parenchyma, levels of total amyloid-β_{40} and amyloid-β_{42} in isolated blood vessels and vessel-depleted cortex were analysed by sandwich ELISAs. The purity of the blood vessel preparation was confirmed by western blot analyses for the enrichment of smooth muscle actin and the relative absence of the neuronal markers microtubule-associated protein-2 and NeuN (Supplementary Fig. 1). Both amyloid-β_{42} ($P = 0.0001$) and amyloid-β_{40} ($P = 0.0001$) accumulated in transgenic mice with age. Whereas there was no difference between the amounts of amyloid-β_{42} in the vessel-depleted cortex versus on the vessels ($P = 0.37$), there was significantly more amyloid-β_{40} deposition on the vessels relative to cortex ($P = 0.0031$) (Table 1). This predominance of amyloid-β_{40} on vessels is in concordance with cerebral amyloid angiopathy composition in patients with Alzheimer's disease (Herzig *et al*., 2006).

Arteriolar tortuosity and radius change

To determine the effect of cerebral amyloid angiopathy development on the morphology of cortical blood vessels *in vivo*, two photon fluorescence microscopy was used to image live cortical vessels in the brains of transgenic and non-transgenic littermates with early, mid- and late-stage cerebral amyloid angiopathy. Since previous studies have utilized pathological markers to demonstrate vessel degeneration (Christie *et al*., 2001; Paul *et al*., 2007), their findings may be confounded by changes in vessel geometry induced during perfusion and fixation. A complete segmentation of the microvascular network in a 3-month-old non-transgenic littermate mouse overlaid on the maximum intensity projection of the corresponding raw data is shown in Fig. 2: the vessels are encoded by their average radius, on a logarithmic scale. Figures 3–5 display the segmentation-derived tubular model of cortical penetrating vessels overlaid on maximum intensity projections of cortical microvasculature at the early, mid and late stage of amyloid-β accumulation in transgenic mice and in the age-matched non-transgenic mice. Arteriolar tortuosity was affected by both transgene ($P < 0.0002$) and age ($P = 0.0043$). Figure 6 shows the arteriolar tortuosity as a function of time in the transgenic versus non-transgenic mice. The transgenic mice had higher arteriolar tortuosity than the non-transgenic mice ($P = 0.0014$); moreover, the arteriolar tortuosity in transgenic mice increased with age ($P = 0.022$). Specifically, arteriolar curvature of the transgenic group was larger than that of non-transgenic cohort at the mid stage ($P = 0.0080$) and trended toward being greater than non-transgenic arteriolar curvature at the late stage ($P = 0.14$). Whereas imaged arteriolar length was not affected by age ($P \sim 0.37$), arteriolar radius tended to decrease with age in the transgenic group ($P = 0.11$) but not in the non-transgenic group ($P = 0.81$). The arteriolar radius of the transgenic group was smaller than that of non-transgenic mice in the mid stage ($P = 0.02$) and trended toward being smaller than the non-transgenic group's radius in the late stage ($P = 0.09$) (Fig. 7). While arteriolar tortuosity did not depend on arteriolar length ($P = 0.56$), higher

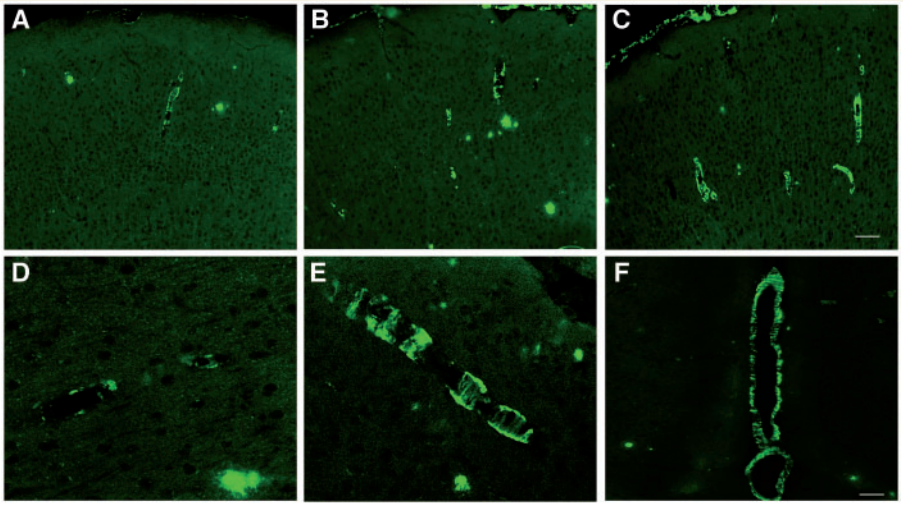

Figure 1 Cortical cerebrovascular amyloid load in the transgenic mice as a function of age. Photomicrographs of cortical tissue sections of transgenic mice demonstrate a significant increase in the number of thioflavin S-positive cortical blood vessels with age: 2-month old (**A**, **D**), 4-month old (**B**, **E**) and 8-month old (**C**, **F**) mice. The extent of vessel amyloid coverage also increases with age (**D–F**). Scale bars: A–C = 75 mm; D–F = 35 mm.

Table 1 Mean amyloid-β_{40} and amyloid-β_{42} accumulation with age on cortex and vessels (pg/ml)

	Early	Mid	Late
Amyloid-β_{40}			
Cortex	0.13 ± 0.08	38.63 ± 11.89	518.89 ± 51.70
Vessel	0.38 ± 0.19	108.36 ± 30.11	1179.23 ± 107.62
Amyloid-β_{42}			
Cortex	0.29 ± 0.13	131.25 ± 15.62	818.81 ± 237.82
Vessel	0.50 ± 0.21	2.95 ± 0.33	751.45 ± 72.17

Mean ± SEM, $n = 6$ for early and for mid, and $n = 5$ for late.

arteriolar tortuosity was associated with smaller arteriolar radius ($P = 0.0012$).

Since vascular amyloid-β deposition was shown to correlate with increased tortuosity in the transgenic mice, we examined the effects of an amyloid-β oligomer-specific treatment on vascular morphology. We utilized prophylactic treatment of transgenic mice with scyllo-inositol to target amyloid-β oligomers *in vivo* (McLaurin *et al.*, 2006). Our results demonstrate that tortuosity was significantly improved after scyllo-inositol treatment of transgenic mice in comparison with untreated transgenic mice ($P = 0.028$), whereas the arteriolar tortuosity of scyllo-inositol-treated transgenic mice was indistinguishable from that of the non-transgenic mice ($P = 0.80$) (Figs 3–5). Moreover, the arteriolar radius of the scyllo-inositol-treated transgenic mice could not be distinguished from that of the non-transgenic mice at any stage ($P_{early} = 0.18$, $P_{mid} = 0.19$, $P_{late} = 0.13$). These results demonstrate that prevention of amyloid-β oligomerization and deposition prevents these morphological vessel changes in the transgenic mice. Previous studies have suggested that the lack of amyloid-β clearance in transgenic mouse models is the result of serum response factor and myocardin-induced down regulation of lipoprotein receptor-related protein 1 in blood vessel walls (Deane *et al.*, 2004; Bell *et al.*, 2009). However, in the TgCRND8 mouse model used in these studies, lipoprotein receptor-related protein 1 expression was not down regulated with disease progression or scyllo-inositol treatment in cortical blood vessels (Supplementary Fig. 2). In agreement, we have previously reported that plasma amyloid-β levels do not significantly change with disease progression or scyllo-inositol treatment further suggesting that normal brain to blood pathways are not altered in this mouse model (McLaurin *et al.*, 2006; Fenili *et al.*, 2007).

In contrast to arteriolar findings, but in concert with arteriolar-specific amyloid-β deposition, venular tortuosity did not change with either age ($P = 0.87$) or transgene and treatment ($P = 0.24$). Venular length was not affected by either transgene and treatment ($P = 0.47$) or age ($P = 0.52$), and likewise, venular radius was unaffected by transgene and treatment ($P = 0.74$) or age ($P = 0.27$).

Microvascular transit time and hypercapnic reactivity are impaired

To determine the effect of vessel tortuosity on vascular function, non-transgenic mice, untreated transgenic and those transgenic treated with scyllo-inositol were assessed for vascular transit times and reactivity to hypercapnia. Vascular transit times were estimated by the amount of time it took a bolus of intravascular fluorescent dye to pass through the vascular network, normalized to the bolus arrival time within the imaged slice place (Stefanovic *et al.*, 2008). Overall, the vascular transit time was significantly affected by state ($P = 0.05$) but not by age ($P = 0.50$). The vascular transit time measurements, in the late stage of amyloid-β accumulation, are shown in Fig. 8A. The transit times in transgenic mice were longer than those of non-transgenic mice ($P = 0.029$),

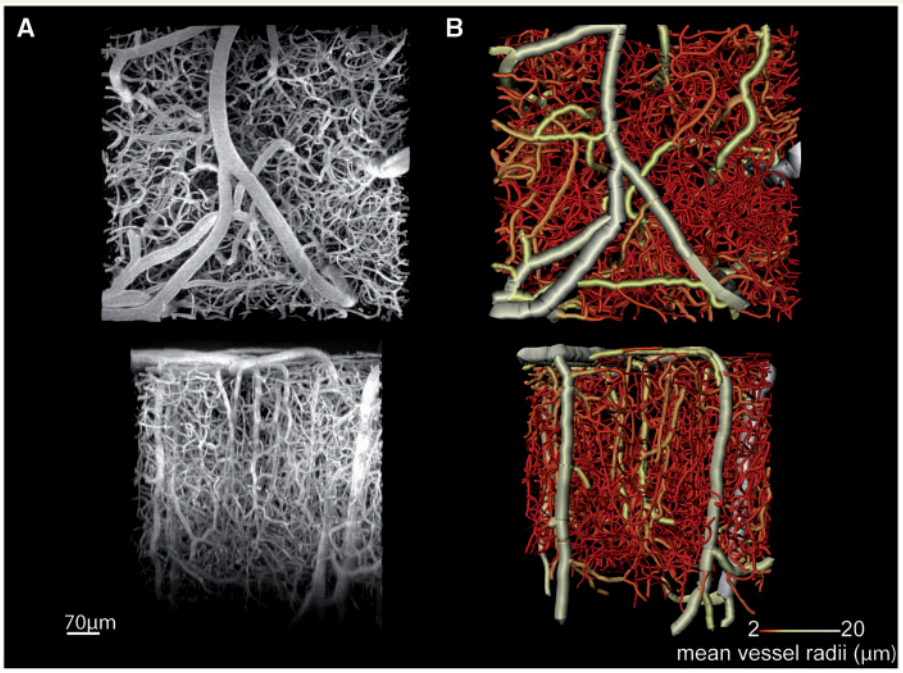

Figure 2 *In vivo* two-photon fluorescence microscopy images of the cortical microcirculation in a 3-month old non-transgenic mouse. Acquired in the primary somatosensory cortex, this maximum intensity projection image (**A**) shows penetrating arterioles running vertically down from the cortical surface (top of the bottom row image) as well as ascending venules interspersed with a dense capillary network. (**B**) A tubular model obtained by segmentation of the branching vessel network shown in (**A**). The colour bar indicates the coding of average vessel diameters. *Top* row images are parallel to the cortical surface, while *bottom* row images are perpendicular to the cortical surface.

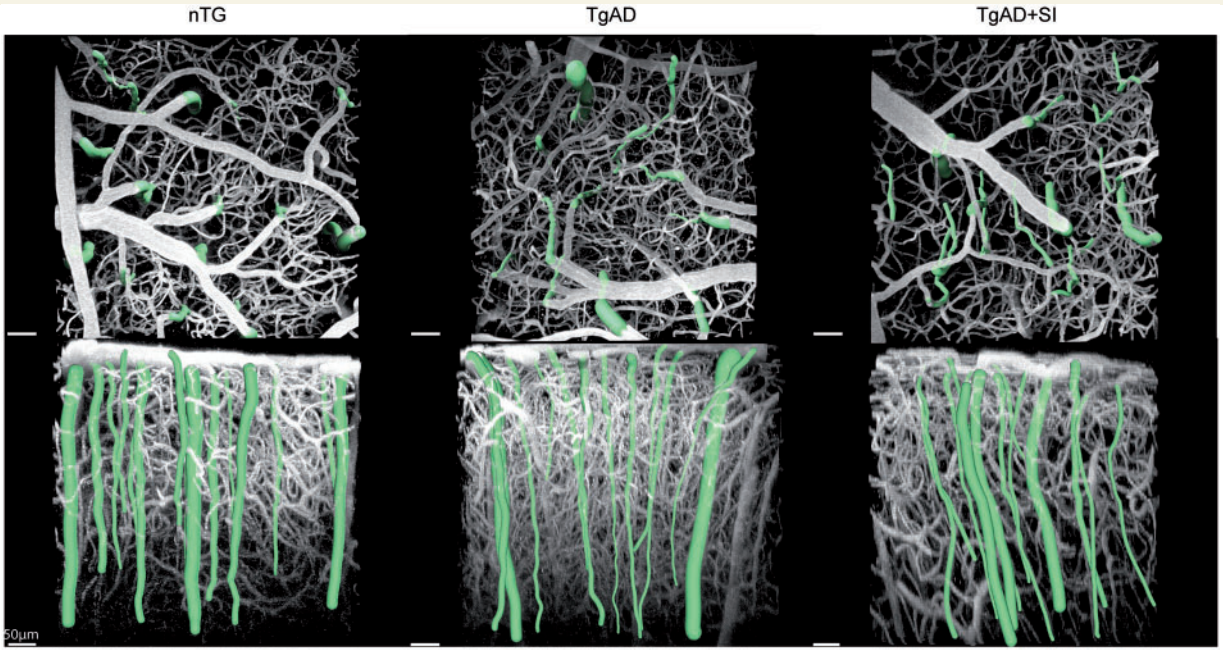

Figure 3 Segmentation of cortical penetrating vessels overlaid on maximum intensity projections of cortical microvasculature at the early time point (2–3 months). Parallel to cortical surface (*top* row) and perpendicular to cortical surface (*bottom* row). Penetrating vessels for each individual mouse are highlighted. Average tortuosity of penetrating vessels for each sample subject (mean ± standard error): non-transgenic (nTG) 1.02 ± 0.003, transgenic (TgAD) 1.04 ± 0.004 and scyllo-inositol-treated transgenic (TgAD + SI) 1.04 ± 0.004.

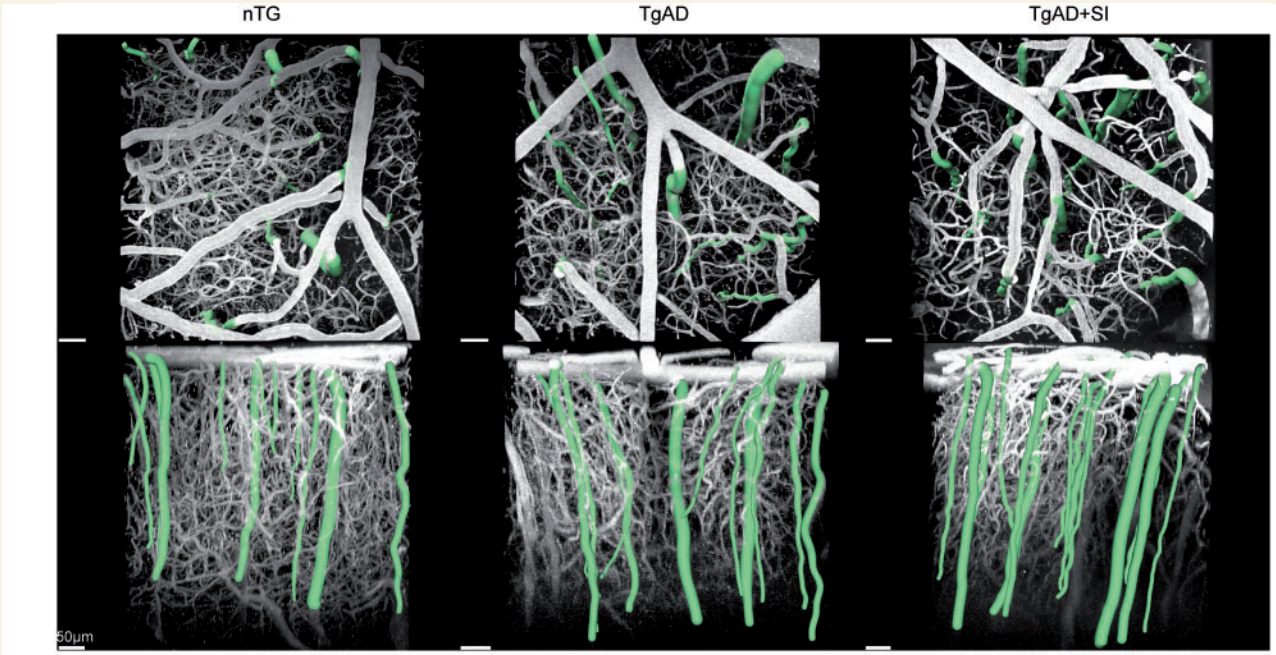

Figure 4 Segmentation of cortical penetrating vessels overlaid on maximum intensity projections of cortical microvasculature at the mid time point (2–3 months): parallel to cortical surface (*top* row) and perpendicular to cortical surface (*bottom* row). Penetrating vessels for each individual mouse are highlighted. Average tortuosity of penetrating vessels for each sample subject (mean ± standard error): non-transgenic (nTG) 1.03 ± 0.004, transgenic (TgAD) 1.06 ± 0.019 and scyllo-inositol-treated transgenic (TgAD + SI) 1.04 ± 0.004.

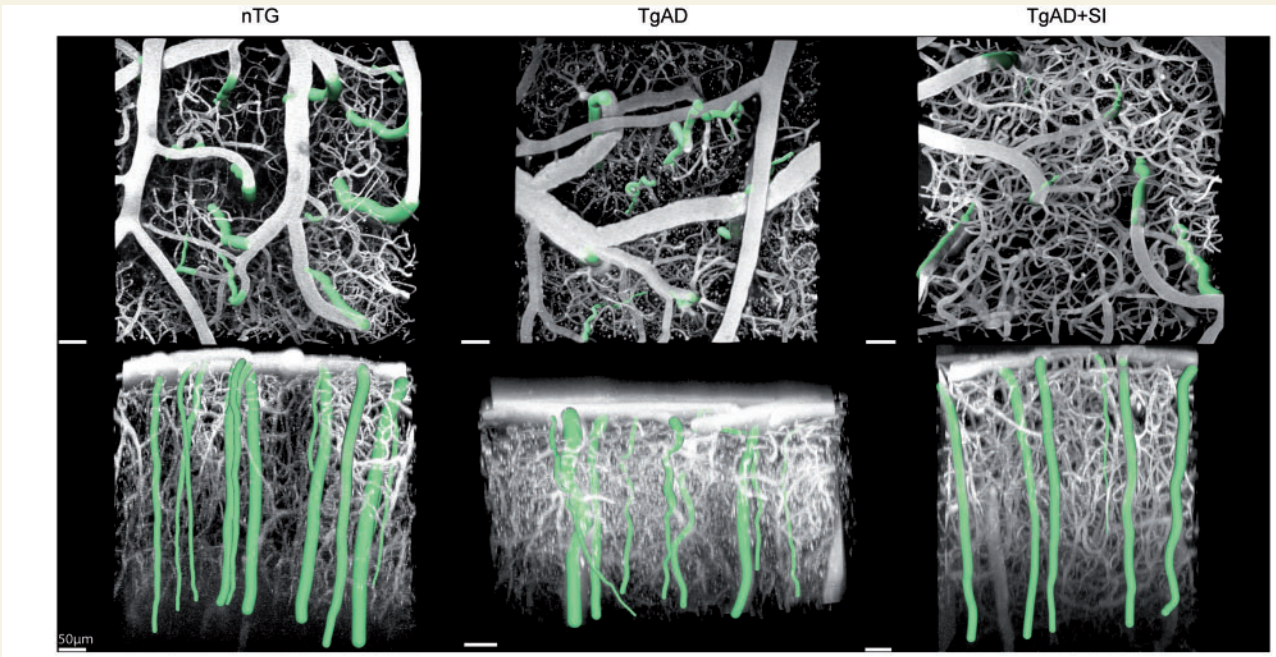

Figure 5 Segmentation of cortical penetrating vessels overlaid on maximum intensity projections of cortical microvasculature at the late time point (6.5–12 months): parallel to cortical surface (*top* row) and perpendicular to cortical surface (*bottom* row). Penetrating vessels for each individual mouse are highlighted. Average tortuosity of penetrating vessels for each sample subject (mean ± standard error): non-transgenic (nTG) 1.03 ± 0.003, transgenic (TgAD) 1.10 ± 0.006 and scyllo-inositol-treated transgenic (TgAD + SI) 1.03 ± 0.005.

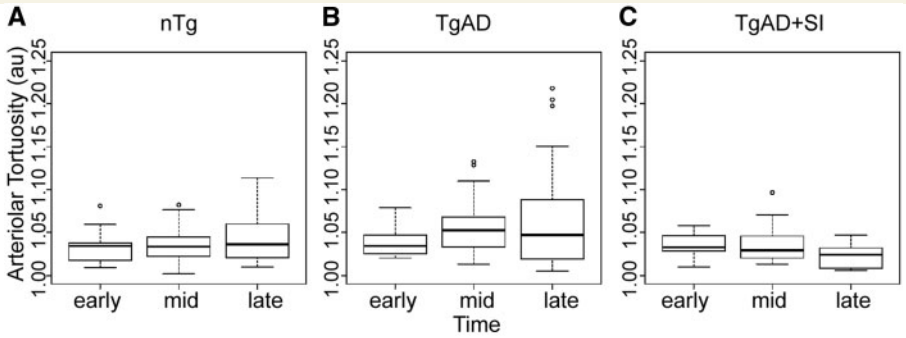

Figure 6 The arteriolar tortuosity as a function of time in non-transgenic (**A**), transgenic (**B**) and scyllo-inositol-treated transgenic (**C**) animals. Transgenic (nTg) mice had higher arteriolar tortuosity than the non-transgenic (TgAD) mice ($P = 0.001$), whereas the scyllo-inositol-treated transgenic (TgAD + SI) mice were indistinguishable from non-transgenic ($P = 0.80$). The arteriolar tortuosity in transgenic mice increased with age ($P = 0.022$): arteriolar curvature of the transgenic was larger than that of non-transgenic at the mid stage ($P = 0.008$) and trended toward being greater than non-transgenic arteriolar curvature at the late stage ($P = 0.14$).

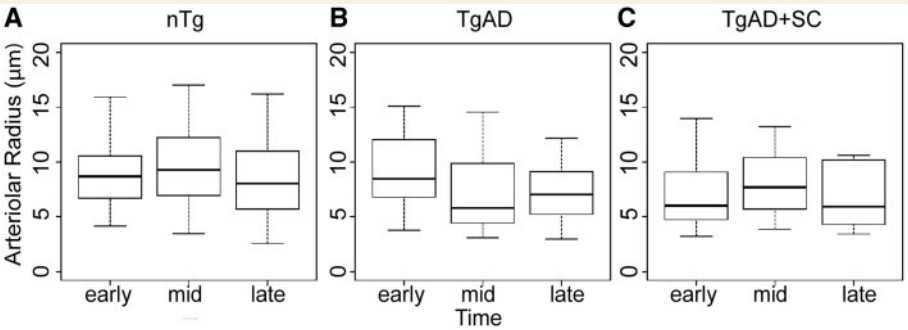

Figure 7 The arteriolar radius as a function of time in non-transgenic (**A**), transgenic (**B**) and scyllo-inositol-treated transgenic (**C**) animals. Arteriolar radius tended to decrease with age in the transgenic (nTg) ($P = 0.11$) but not in non-transgenic (TgAD) ($P = 0.81$) or scyllo-inositol-treated transgenic (TgAD + SI) ($P = 0.74$). The arteriolar radius of the transgenic was smaller than that of non-transgenic in the mid stage ($P = 0.02$) and trended toward being smaller than the non-transgenic group's radius in the late stage ($P = 0.09$).

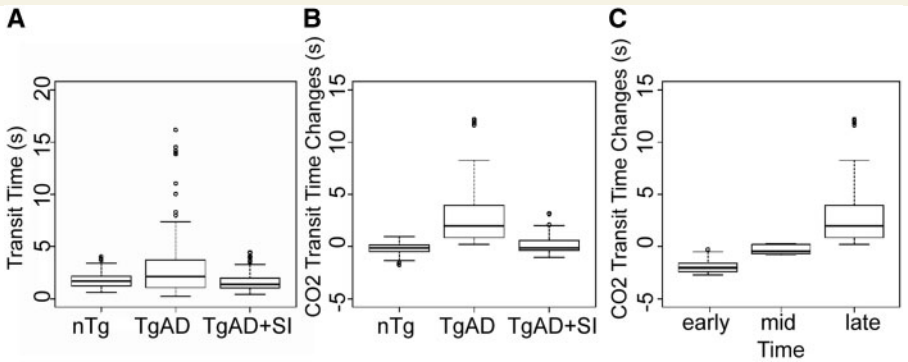

Figure 8 (**A**) The transit time (in s) across the different groups, at the late stage. The transit time was both longer ($P = 0.029$) and more variable in the transgenic (nTg) group ($P < 2.2 \times 10^{-16}$) when compared to non-transgenic (TgAD) group. The scyllo-inositol-treated transgenic (TgAD + SI) group transit times could not be distinguished from the non-transgenic ones ($P = 0.82$). (**B**) The hypercapnia induced changes in the absolute transit time across the different groups, at the late stage. Whereas the hypercapnia induced transit time shortening in non-transgenic animals ($P = 0.031$), it resulted in transit time elongation in transgenic mice ($P = 0.0001$). (**C**) The hypercapnia induced changes in the absolute transit time in the transgenic group, across time. With age, the transit time in the transgenic group tended to increase ($P = 0.12$).

whereas scyllo-inositol-treated transgenic mice transit times were not distinguishable from those of non-transgenic mice ($P = 0.82$). The transit time dispersion, taken to reflect the efficiency of the microvascular network (lower dispersion being a putative marker of a more efficient vascular network), was higher in the transgenic group, relative to that in non-transgenic, during both air breathing ($P = 0.039$) and hypercapnia ($P = 0.030$). In contrast, scyllo-inositol-treated transgenic transit time dispersion was not distinguishable from non-transgenic during either air breathing ($P = 0.8787$) or hypercapnia ($P = 0.6597$). These data suggest that the transgenic vasculature is functionally inefficient as reflected in the larger dispersion of transit times in the transgenic mice. Furthermore, prevention of amyloid-β aggregation and deposition by scyllo-inositol is shown to successfully resolve this impairment.

The hypercapnic challenge had a significant effect on vascular transit times across the three groups ($P = 0.0003$), as shown in Fig. 8B. In the non-transgenic group, hypercapnia induced the expected transit time shortening ($P = 0.031$) as a result of carbon-dioxide-induced vessel dilatation. In contrast, the hypercapnic challenge resulted in transit time elongation in the transgenic group ($P = 0.0001$). Figure 8C displays the hypercapnia-induced changes in the transit time in the transgenic group, across time. There was a strong trend toward carbon dioxide-induced transit time increase with amyloid-β accumulation in the transgenic animals ($P = 0.12$). Given the previously discussed changes in arteriolar, but not venular vascular networks and the preferential accumulation of amyloid-β on the arterioles over venules (Weller and Nicoll, 2003; Shin *et al*., 2007; Serrano-Pozo *et al*., 2011; Fig. 9), we hypothesize that this paradoxical response to hypercapnia resulted from compromised carbon-dioxide-induced dilatation of the supply vasculature in the presence of preserved carbon-dioxide-elicited venous dilatation; the increase in the drainer calibre alone thus elicited elongation of the vascular transit time upon hypercapnia, providing further evidence of the profound compromise of vascular function in this transgenic mouse model.

Discussion

In recent years, the vascular compromise in Alzheimer's disease dementia has garnered increased research attention. Amyloid-β peptides have been demonstrated to elicit vasoconstriction and cause vascular degeneration, elevating the risk of haemorrhage and stroke (Perlmutter, 1994; Miao *et al.,* 2005; Tian *et al*., 2006). While the significance of vascular dysfunction has thus become widely appreciated, the pathogenesis of cerebral amyloid angiopathy and its implications have yet to be fully elucidated. In the present work, we examined, *in situ*, the changes in cortical penetrating vessel morphology and function with progressive

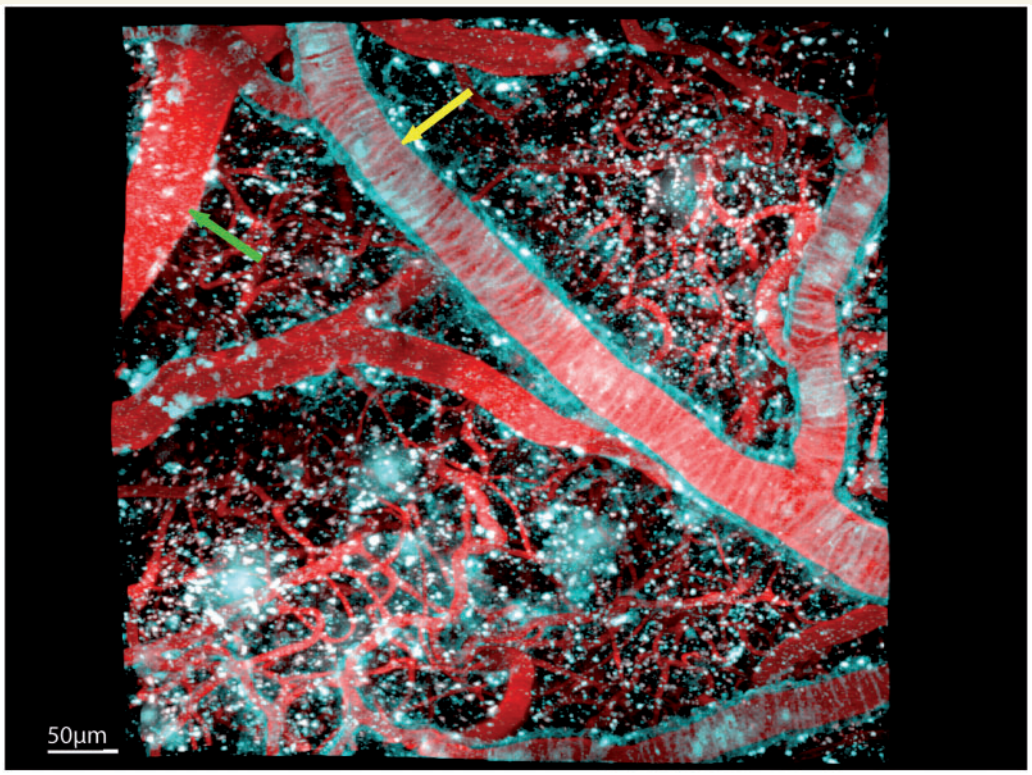

Figure 9 Maximum intensity projection image of the cortical microvasculature in a 9.5-month-old transgenic mouse. The autofluorescence signal is shown in blue (false coloured), with the intravascular fluorophore signal displayed in red. Cerebral amyloid angiopathy appears as striped rings around the arterioles (yellow arrow); this ring pattern is not present around the venules (green arrow). The vessels have been categorized based on the bolus arrival time estimates from the bolus tracking data, venules showing delayed bolus arrivals relative to arterioles.

accumulation of amyloid-β in the TgCRND8 mouse model of Alzheimer's disease. Under physiological conditions, cortical penetrating arterioles have been shown to be key for the healthy supply of the cortex with metabolites (Nishimura *et al.,* 2007) and clearance of toxins, such as amyloid-β, from the brain (Nicoll *et al*., 2004). In TgCRND8 mice, we found the progressive accumulation of amyloid-β_{42} and particularly amyloid-β_{40} associated with transgene-dependent increase in the tortuosity of the penetrating arterioles, with the largest change observed in mid-stage of the disease followed by the saturation of this effect in the later stage. At the same time, the intraluminal arteriolar radii have been shown to progressively decrease, probably exacerbating the impairment of the normal cortical blood supply. These effect sizes are consistent with the morphological changes reported in the quantitative examinations of Alzheimer's disease patient microvascular beds (Fischer *et al*., 1990; Thore *et al.,* 2007). In concert with earlier reports of preferential deposition of amyloid-β on arteriolar over venular walls (Weller and Nicoll, 2003; Shin *et al*., 2007; Serrano-Pozo *et al*., 2011), we observed neither tortuosity nor calibre changes in the venules. Moreover, we found these morphological changes accompanied by progressive compromise of the microvascular function. The latter was reflected in a greater variability in vascular transit times across the cortical microvasculature of the transgenic mice, longer vascular transit times and impaired response of the microvascular bed to the global vasodilatory challenge posed by elevated carbon dioxide content in the inspired gas mixture. Transgenic mice not only showed a progressive compromise in hypercapnia-induced vascular reactivity, but also exhibited transit time elongation rather than shortening in response to hypercapnia in the late stage of the disease. We believe this paradoxical hypercapnic response results from differential effects of the disease process on arteriolar versus venular side of the microvascular network, with largely preserved carbon dioxide-induced venular vasodilatation accompanying a profoundly compromised arteriolar dilatation.

We have previously shown that scyllo-inositol, administered post-weaning, rescues the age-progressive accumulation of amyloid-$\beta_{40/42}$ in both parenchyma and on blood vessels in this transgenic model (McLaurin *et al.,* 2006). We presently found that administration of scyllo-inositol resolved the vascular morphological and functional changes observed in the transgenic mice. The scyllo-inositol-treated TgCRND8 mice were thus found to be indistinguishable from their non-transgenic littermates with respect to arteriolar tortuosity, arteriolar calibre, transit time dispersion and vascular reactivity to hypercapnia. These data thus provide evidence that the vascular impairment in the TgCRND8 mice is consequent to amyloid-β accumulation as both soluble oligomers and insoluble deposits and that these structural and functional compromises of the cortical microvasculature may be resolved by preventing amyloid-β oligomerization and/or fibrillization. Since scyllo-inositol decreases both soluble and insoluble amyloid-β levels, the compromise in vascular function may be related not only to the development of cerebral amyloid angiopathy but also to amyloid-β-induced vasoactivity, endothelial and pericyte damage or oxidative stress (Thomas *et al*., 1996; Verbeek *et al*., 1997; Butterfield, 2002; Carrano *et al*., 2011).

Of note, in contrast to previous reports (Deane *et al*., 2004; Bell *et al*., 2009), we did not find a disease-associated decrease in lipoprotein receptor-related protein 1 expression in isolated cortical blood vessels nor changes in plasma amyloid-β levels, suggesting that brain to plasma efflux pathways are unaffected in this mouse model. Hence, accumulation of amyloid-β and development of cerebral amyloid angiopathy observed in this model may result from decreased microvascular function and motive force for effective perivascular amyloid-β drainage (Weller *et al.,* 2009). In addition, in light of the recent anti-amyloid-β immunization studies that reported strong associations between reduced parenchymal plaque load and increased cerebral amyloid angiopathy severity and brain microhaemorrhages (Boche *et al*., 2008), we inspected the two photon fluorescent data on the microvascular architecture in the scyllo-inositol-treated animals at each stage for indication of fluorescent dextran extravasation. We did not, however, observe any such occurrences, arguing against an increase in bleeding from cortical microvessels subsequent to scyllo-inositol treatment.

Overall, this work reports on the implications of cerebral amyloid angiopathy on the morphology and function of brain microvessels over the course of disease progression, measured by *in vivo* two photon fluorescence microscopy so as to avoid confounds from tissue processing techniques. Our findings shed new light on the correlation between amyloid-β accumulation and microvascular impairment in the Alzheimer's disease brain, underscore the importance of cerebral amyloid angiopathy in the aetiology of Alzheimer's disease and demonstrate the resolution of the progressive structural and functional impairment of the brain microvasculature by prevention of amyloid-β aggregation and deposition. The translation of our results remains to be determined as mouse models of Alzheimer's disease do not recapitulate all aspects of the disease process nor the normal ageing-associated changes seen in humans.

Acknowledgements

We thank Jianfei He and Kun Zhang for the surgical work as well as Lynsie Thomason for technical support.

Funding

Sunnybrook Research Institute and the Canadian Institutes of Health Research (MOP-37857 to J.M., MOP-94376 to J.M., C.A.H., and B.S. and MOP-10246 to J.M. and B.S.). A.D., B.S., L.V.C., M.E.B., A.Y.L., K.M., C.A.H., and B.S. declare no conflict of interest. J.M. is named inventor on patents and patent applications relating to scyllo-inositol.

Supplementary material

Supplementary material is available at *Brain* online.

References

Bell RD, Deane R, Chow N, Long X, Sagare A, Singh I, et al. SRF and myocardin regulate LRP-mediated amyloid-β clearance in brain vascular cells. Nat Cell Biol 2009; 11: 143–53.

Boche D, Zotova E, Weller RO, Love S, Neal JW, Pickering RM, et al. Consequence of A immunization on the vasculature of human Alzheimer's disease brain. Brain 2008; 131: 3299–310.

Bullitt E, Gerig G, Pizer SM, Lin W, Aylward SR. Measuring tortuosity of the intracerebral vasculature from MRA images. IEEE Trans Med Imaging 2003; 22: 1163–71.

Butterfield DA. Amyloid-β-peptide (1–42)-induced oxidative stress and neurotoxicity: implications for neurodegeneration in Alzheimer's disease brain. A review. Free Radic Res 2002; 36: 1307–13.

Carrano A, Hoozemans JJM, van der Vies SM, Rozemuller AJM, van Horssen J, de Vries HE. Amyloid beta induces oxidative stress-mediated blood–brain barrier changes in capillary amyloid angiopathy. Antioxid Redox Signal 2011; 15: 1167–78.

Chishti MA, Yang DS, Janus C, Phinney AL, Horne P, Pearson J, et al. Early-onset amyloid deposition and cognitive deficits in transgenic mice expressing a double mutant form of amyloid precursor protein 695. J Biol Chem 2001; 276: 21562–70.

Choi JK, Carreras I, Dedeoglu A, Jenkins BG. Consequence of Aβ immunization on the vasculature of human Alzheimer's disease brain. Neuropharmacology 2010; 59: 353–7.

Christie R, Yamada M, Moskowitz M, Hyman B. Structural and functional disruption of vascular smooth muscle cells in a transgenic mouse model of amyloid angiopathy. Am J Pathol 2001; 158: 1065–71.

Citron M. Alzheimer's disease: treatments in discovery and development. Nat Neurosci 2002; 5 (Suppl): 1055–7.

Collie A, Maruff P. The neuropsychology of preclinical Alzheimer's disease and mild cognitive impairment. Neurosci Biobehav Rev 2000; 24: 365–74.

Deane R, Wu Z, Sagare A, Davis J, Yan SD, Hamm K, et al. LRP/Amyloid-β-peptide interaction mediates differential brain efflux of A-β-isoforms. Neuron 2004; 43: 333–44.

Duvernoy HM, Delon S, Vannson JL. Cortical blood vessels of the human brain. Brain Res Bull 1981; 7: 519–79.

Fenili D, Brown ME, Rappaport RV, McLaurin J Properties of scyllo-inositol as a therapeutic treatment of AD-like pathology. J Mol Med 2007; 85: 603–12.

Fenili D, Weng YQ, Aubert I, Nitz M, McLaurin J. Sodium/myo-inositol transporters: an examination of substrate transport requirements and regional brain expression in the TgCRND8 mouse model of Alzheimer's disease. PLoS One 2011; 6: e24032.

Fischer VW, Siddiqi A, Yusufaly Y. Altered angioarchitecture in selected areas of brains with Alzheimer's disease. Acta Neuropathol 1990; 79: 672–9.

Girouard H, Iadecola C. Neurovascular coupling in the normal brain and in hypertension, stroke, and Alzheimer disease. J Appl Physiol 2006; 100: 328–35.

Greenberg SM. Cerebral amyloid angiopathy and vessel dysfunction. Cerebrovasc Dis 2002; 13 (Suppl 2): 42–47.

Han BH, Zhou M-l, Abousaleh F, Brendza RP, Dietrich HH, Koenigsknecht-Talboo J, et al. Cerebrovascular dysfunction in amyloid precursor protein transgenic mice: contribution of soluble and insoluble amyloid-β peptide, partial restoration via γ-secretase inhibition. J Neurosci 2008; 28: 13542–50.

Hawkes CA, McLaurin J. Selective targeting of perivascular macrophages for clearance of beta-amyloid in cerebral amyloid angiopathy. PNAS 2009; 106: 1261–6.

Herzig MC, Van Nostrand WE, Jucker M. Mechanism of cerebral beta-amyloid angiopathy: murine and cellular models. Brain Pathol 2006; 6: 40–54.

Holland CM, Smith EE, Csapo I, Gurol ME, Brylka DA, Killiany RJ, et al. Spatial distribution of white-matter hyperintensities in Alzheimer disease, cerebral amyloid angiopathy, and healthy aging. Stroke 2008; 39: 1127–33.

Hunter JM, Kwan J, Malek-Ahmadi M, Maarouf CL, Kokjohn TA, Belden C, et al. Morphological and pathological evolution of the brain microcirculation in aging and Alzheimer's disease. Plos ONE 2012; 7: e36893.

Kalaria RN. Cerebral vessels in ageing and Alzheimer's disease. Pharmacol Ther 1996; 72: 193–214.

Kalaria RN. Small vessel disease and Alzheimer's dementia: pathological considerations. Cerebrovasc Dis 2002; 13 (Suppl2): 48–52.

Kasischke KA, Lambert EM, Panepento B, Sun A, Gelbard HA, Burgess RW, et al. Two-photon NADH imaging exposes boundaries of oxygen diffusion in cortical vascular supply regions. J Cereb Blood Flow Metab 2011; 31: 68–81.

Kershaw L, Cheng H. A general dual-bolus approach for quantitative DCE-MRI. Magn Reson Imaging 2011; 29: 160–6.

Kim J, Leira E, Callison R, Ludwig B, Moritani T, Magnotta V, et al. Toward fully automated processing of dynamic susceptibility contrast perfusion MRI for acute ischemic cerebral stroke. Comput Methods Programs Biomed 2010; 98: 204–13.

Kwan AC, Duff K, Gouras GK, Webb WW. Optical visualization of Alzheimer's pathology via multiphoton-excited intrinsic fluorescence and second harmonic generation. Opt Express 2009; 17: 3679–89.

LeVine H III. Small molecule inhibitors of Abeta assembly. Amyloid 2007; 14: 185–97.

Lindvere L, Dorr A, Stefanovic B. Two-photon fluorescence microscopy of cerebral hemodynamics. Cold Spring Harb Protoc 2010 (9):pdb.prot5494.

Ma K, Mount HT, McLaurin J. Region-specific distribution of β-amyloid peptide and cytokine expression in TgCRND8 mice. Neurosci Lett 2011; 492: 5–10.

McLaurin J, Golomb R, Jurewicz A, Antel JP, Fraser PE. Inositol stereoisomers stabilize an oligomeric aggregate of Alzheimer amyloid beta peptide and inhibit abeta-induced toxicity. J Biol Chem 2000; 275: 18495–502.

McLaurin J, Kierstead ME, Brown ME, Hawkes CA, Lambermon MH, Phinney AL, et al. Cyclohexanehexol inhibitors of Abeta aggregation prevent and reverse Alzheimer phenotype in a mouse model. Nat Med 2006; 12: 801–8.

Miao J, Xu F, Davis J, Otte-Höller I, Verbeek MM, Van Nostrand WE. Cerebral microvascular amyloid beta protein deposition induces vascular degeneration and neuroinflammation in transgenic mice expressing human vasculotropic mutant amyloid beta precursor protein. Am J Pathol 2005; 167: 505–15.

Nicolakakis N, Hamel E. Neurovascular function in Alzheimer's disease patients and experimental models. J Cereb Blood Flow Metab 2011; 31: 1354–70.

Nicoll JA, Yamada M, Frackowiak J, Mazur-Kolecka B, Weller RO. Cerebral amyloid angiopathy plays a direct role in the pathogenesis of Alzheimer's disease. Pro-CAA position statement. Neurobiol Aging 2004; 25: 589–97.

Nishimura N, Schaffer CB, Friedman B, Lyden PD, Kleinfeld D. Penetrating arterioles are a bottleneck in the perfusion of neocortex. Proc Natl Acad Sci USA 2007; 104: 365–70.

Paul J, Strickland S, Melchor JP. Fibrin deposition accelerates neurovascular damage and neuroinflammation in mouse models of Alzheimer's disease. J Exp Med 2007; 204: 1999–2008.

Perlmutter LS. Microvascular pathology and vascular basement membrane components in Alzheimer's disease. Mol Neurobiol 1994; 9: 33–40.

Pfeifer LA, White LR, Ross GW, Petrovitch H, Launer LJ. Cerebral amyloid angiopathy and cognitive function: The HAAS autopsy study. Neurology 2002; 58: 1629–34.

Pinheiro JC, Bates DM. Mixed-effects models in S and S-PLUS. New York: Springer; 2000.

Querfurth HW, LaFerla FM. Alzheimer's disease. N Engl J Med 2010; 362: 329–44.

Scharrer E. Arteries and veins in the mammalian brain. Anat Rec 1940; 78: 173–96.

Serrano-Pozo A, Frosch MP, Masliah E, Hyman BT. Neuropathological alterations in Alzheimer disease. Cold Spring Harb Perspect Med 2011; 1: a006189.

Shin HK, Jones PB, Garcia-Alloza M, Borrelli L, Greenberg SM, Bacskai BJ, et al. Age-dependent cerebrovascular dysfunction in a transgenic mouse model of cerebral amyloid angiopathy. Brain 2007; 130 (Pt 9): 2310–19.

Stefanovic B, Hutchinson E, Yakovleva V, Schram V, Russell JT, Belluscio L, et al. Functional reactivity of cerebral capillaries. J Cereb Blood Flow Metab 2008; 28: 961–72.

Takano T, Han X, Deane R, Zlokovic B, Nedergaard M. Two-photon imaging of astrocytic Ca2 + signaling and the microvasculature in experimental mice models of Alzheimer's disease. Ann NY Acad Sci 2007; 1097: 40–50.

Thomas T, Thomas G, McLendon C, Sutton T, Mullan M. β-amyloid-mediated vasoactivity and vascular endothelial damage. Nature 1996; 380: 168–71.

Thore CR, Anstrom JA, Moody DM, Challa VR, Marion MC, Brown WR. Morphometric analysis of arteriolar tortuosity in human cerebral white matter of preterm, young, and aged subjects. J Neuropathol Exp Neurol 2007; 66: 337–45.

Tian J, Shi J, Smallman R, Iwatsubo T, Mann DM. Relationships in Alzheimer's disease between the extent of Abeta deposition in cerebral blood vessel walls, as cerebral amyloid angiopathy, and the amount of cerebrovascular smooth muscle cells and collagen. Neuropathol Appl Neurobiol 2006; 32: 332–40.

Townsend M, Cleary JP, Mehta T, Hofmeister J, Lesne S, O'Hare E, et al. Orally available compound prevents deficits in memory caused by the Alzheimer amyloid-beta oligomers. Ann Neurol 2006; 60: 668–76.

Verbeek MM, De Waal RM, Schipper JJ, Van Nostrand WE. Rapid degeneration of cultured human brain pericytes by amyloid beta protein. J Neurochem 1997; 68: 1135–41.

Weller RO, Nicoll JA. Cerebral amyloid angiopathy: pathogenesis and effects on the ageing and Alzheimer brain. Neurol Res 2003; 25: 611–6.

Weller RO, Preston SD, Subash M, Carare RO. Cerebral amyloid angiopathy in the aetiology and immunotherapy of Alzheimer disease. Alzheimer's Res Ther 2009; 1: 6(doi:10.1186/alzrt6).